1961

Orientation effects on the rubidium magnetometer.

Woodall, Franklin Thomas

Monterey, California: U.S. Naval Postgraduate School

ORIENTATION EFFECTS ON THE RUBIDIUM MAGNETOMETER

FRANKLIN THOMAS WOODALL, JR.

ORIENTATION EFFECTS ON THE RUBIDIUM MAGNETOMETER

* * * * * * *

Franklin Thomas Woodall Jr.

ORIENTATION EFFECTS ON THE RUBIDIUM MAGNETOMETER

by

Franklin Thomas Woodall Jr.
Lieutenant, United States Navy

Submitted in partial fulfillment of
the requirements for the degree of

MASTER OF SCIENCE
IN
ENGINEERING ELECTRONICS

United States Naval Postgraduate School
Monterey, California

1 9 6 1

U. S. Naval Postgraduate School
Monterey, California

ORIENTATION EFFECTS ON THE RUBIDIUM MAGNETOMETER

by

Franklin Thomas Woodall Jr.
Lieutenant, United States Navy

This work is accepted as fulfilling

the thesis requirements for the degree of

MASTER OF SCIENCE

IN

ENGINEERING ELECTRONICS

from the

United States Naval Postgraduate School

ABSTRACT

This paper is an attempt to provide an insight into the rather complicated problem of heading error in spin-resonance magnetometers. The particular system investigated is the self oscillating rubidium vapor magnetometer. Theory is developed which shows the magnitude of heading error to be a function of many parameters; however, only two of these parameters, the optical pumping rate and the r-f feedback, are singled out for experimental varification. The results are encouraging in that they show that the magnitude of heading error follows a definite pattern; consequently, it should be possible to introduce compensating networks to reduce or possibly eliminate entirely the orientation effects.

The material for this paper was gathered while the author was a guest of Varian Associates in Palo Alto, California. Thanks are expressed to the staff of the instrument division, and especially to Dr. J. A. Arnold, for their suggestions and technical help.

The writer also wishes to thank Professor Carl E. Menneken of the U. S. Naval Postgraduate School for his constructive criticisms in the preparation of this paper.

TABLE OF CONTENTS

LIST OF ILLUSTRATIONS

LIST OF ILLUSTRATIONS (cont'd)

I. INTRODUCTION

Precision magnetic field measurements are being used in an increasing number of military, scientific, and industrial applications. Many of these applications are such that the measurements must be obtained from a moving platform. This means that the instrument used must be compact; it must be rugged enough to sustain forces such as those encountered when launching or recovering satellites; it must use little power; and it must be more sensitive than existing operational devices.

The recently developed rubidium vapor, spin-resonance, magnetometer meets these requirements. It has already been flown as part of the instrument package in several satellites and its performance met or exceeded expectations. It is anticipated that the magnetometer will perform equally well in the military applications for which it is presently being packaged.

Like most new devices, there are engineering problems that must be solved before the magnetometer is completely operational. The one with which this paper is concerned is heading error- the variation of field strength reading as the orientation of the magnetometer is changed. It will be shown that the orientation effects are fundamental to spin-resonance magnetometers using an absorption media having nuclear spin other than zero. It will also be shown that, to some extent, the magnitude of the heading error is a function of design parameters which may be altered to suit a specific application of the instrument.

II. THEORY

The particular magnetometer to be discussed is an oscillator whose frequency is determined by the energy difference between the Zeeman split, hyperfine levels of the 5s state of the rubidium 85 atom. This energy difference is in turn determined by the magnitude of an external magnetic field, in this case the earth's field. By utilizing appropriate techniques to measure the oscillator frequency, absolute field measurements to a few gamma, or field perturbations to .01 gamma may be made. To describe the operation, it will be necessary to investigate the techniques used to perform the basic operating steps of aligning and tipping the nuclear magnetic moments, and then detecting and measuring the resulting precession frequency.

A. Alignment of the Nuclear Magnetic Moments

The alignment of the magnetic moments is accomplished by utilizing the optical pumping techniques described by Kastler[1]. A pyrex cell containing rubidium vapor is irradiated with the light from an excited rubidium lamp. Normally this stimulates transitions out of the S to the P states corresponding to the quantum mechanical restriction $\Delta m = \pm 1$. By using circularily polarized light, however, the transitions can be restricted to either $\Delta m = +1$ or $\Delta m = -1$ depending on the sense of circular polarization[2]. For light polarized such that $\Delta m = +1$, the transition

[1] A. Kastler, Proc. Phys. Soc., A67, 863 (1954)

[2] G. Herzberg, Atomic Spectra and Atomic Structure

probabilities out of the various sublevels of the ground state have been calculated and are tabulated in Fig. 1. Atoms in excited states return almost immediately to the ground state by emission of a photon. Since the return transition is not restricted to $\Delta m = +1$ and since there is considerable mixing in the excited $^2P_{1/2}$ and $^2P_{3/2}$ levels, (a condition that may be enhanced by the addition of a buffer gas), the return to the ground state is random. It is apparent then that at some time, T_P, the upper levels of F=3 and, to a smaller extent, the lower levels of F=2 will be over populated, while the lower levels of F=3 and upper levels of F=2 will be nearly depleted.

F	m	$^2S_{1/2} \rightarrow {}^2P_{1/2}$
3	3	0
	2	1
	1	2
	0	3
	-1	4
	-2	5
	-3	6
2	-2	5
	-1	4
	0	3
	1	2
	2	1

FIG. 1
TRANSITION PROBABILITIES OUT OF THE $^2S_{1/2}$ TO THE $^2P_{1/2}$ STATE WITH THE QUANTUM MECHANICAL RESTRICTION $\Delta m = +1$

The optical pumping process is illustrated in Fig's 2 and 3. A model having zero nuclear spin is used for the illustrations in order to avoid the confusing complexity of the actual R_b 85 energy level diagram,

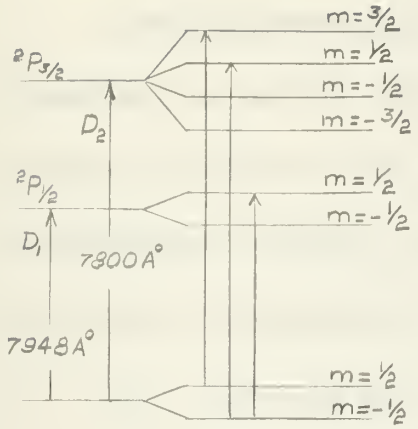

FIG. 2
TRANSITIONS OUT OF THE $^2S_{1/2}$ STATE ASSUMING ZERO NUCLEAR SPIN AND WITH THE RESTRICTION $\Delta m = +1$

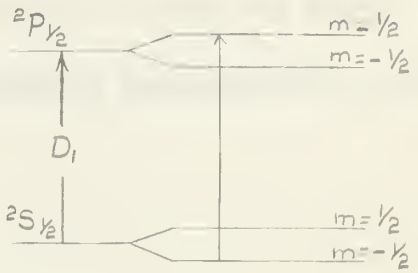

FIG. 3
TRANSITIONS OUT OF THE $^2S_{1/2}$ STATE WHEN THE D_2 LINE IS FILTERED

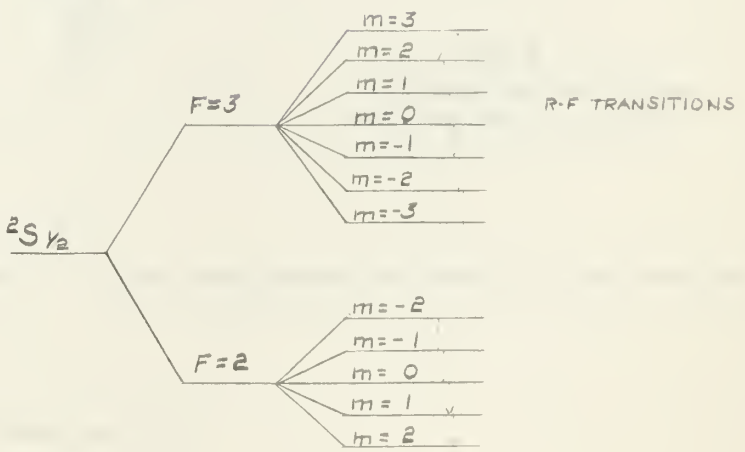

FIG. 4
ENERGY LEVEL DIAGRAM OF THE GROUND STATE OF Rb 85 IN A WEAK MAGNETIC FIELD

however, the principles involved are basically the same. Fig. 4 is the actual energy level diagram of the ground state and shows the field dependent radio frequency transitions.

The time necessary to complete the pumping process, T_p, will be dependent not only on the intensity of the light source, but also on the degree to which the light, as viewed parallel to the earth's field $\bar{H}_o$, is elliptically polarized. Right hand circularily polarized light may be described by the equations:

(1) $P_x = A \cos \omega t$

$P_y = A \sin \omega t$

Referring to Fig. 5, if the circularily polarized source is rotated with respect to $\bar{H}_o$, the observer now sees elliptically polarized light.

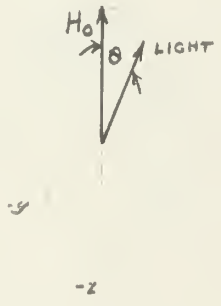

FIG. 5
ROTATION OF LIGHT AXIS
WITH RESPECT TO $\bar{H}_o$

Thus, for any angle, θ, the polarization as seen by the observer is described by

(2) $P_x = A \cos\theta \cos \omega t$

$P_y = A \sin \omega t$

From (2) it is apparent that the degree of light polarization has a $\cos\theta$ variation, and for $\theta = 90^o$, the polarization is linear and no optical pumping is achieved. Since the signal to noise ratio of the output is dependent on the extent to which the sample is pumped, the sensitivity

will also have a cos θ dependence. The plane, $\theta = 90^{\circ}$, is referred to as the equatorial dead zone.

Note that had $\bar{H}_o$ been rotated and the light orientation held fixed, the results would have been identical.

B. Spin Displacement

The result thus far has been to produce a net alignment of the individual nuclear magnetic moments, $\bar{\mu}_{Fi}$, at an angle to $\bar{H}_o$ dictated by quantum energy considerations. The magnetic vectors associated with $\bar{\mu}_{Fi}$ precess around $\bar{H}_o$ in an incoherent manner such that if a total magnetization vector, $\bar{M}$, is defined where $\gamma\bar{M} = \sum_{i=1}^{N} \bar{\mu}_{Fi}$; then

$$\bar{M} = M_x \bar{i} + M_y \bar{j} + M_z \bar{k} \tag{3}$$

and in this case $M_x = M_y = 0$. The purpose of this section is to show how $\bar{M}$ is tipped with respect to $\bar{H}_o$, and subsequently precesses about $\bar{H}_o$ at the Larmor precession frequency.

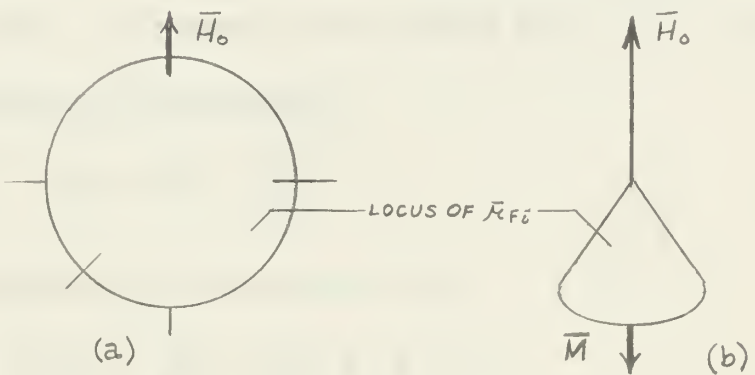

FIG. 6

(a) LOCUS OF $\bar{\mu}_{Fi}$ BEFORE OPTICAL PUMPING (NEGLECTING THE SMALL EFFECT OF BOLTZMAN DISTRIBUTION) (b) ALIGNMENT OF $\bar{\mu}_{Fi}$ AND RESULTANT $\bar{M}$ DUE TO OPTICAL PUMPING

If $\bar{M}$ is initially assumed to be displaced from $\bar{H}_o$ by an angle, α, a torque given by $\frac{d\bar{M}}{dt} = \gamma\bar{M} \times \bar{H}_o$ will be produced, with the resulting rotation in a plane perpendicular to both $\bar{M}$ and $\bar{H}_o$.

Now assume a coordinate system rotating with angular velocity $-\bar{\omega}$.[3]

With respect to this new coordinate system

$$(4) \quad \frac{\partial \bar{M}}{\partial t} = \frac{d\bar{M}}{dt} + (\bar{\omega} \times \bar{M})$$
$$= (\gamma \bar{M} \times \bar{H}_o) + \left(\frac{\bar{\omega}}{\gamma} \times \gamma \bar{M}\right)$$
$$= \gamma \bar{M} \times \left(\bar{H}_o - \frac{\bar{\omega}}{\gamma}\right)$$

where $\bar{H}_o - \frac{\bar{\omega}}{\gamma}$ is the effective field and is stationary when viewed in the rotating frame.

Thus the requirement that $\bar{M}$ be displaced from $\bar{H}_o$ is clearly illustrated, and a method of maintaining this displacement against the pumping action of the rubidium lamp is suggested. Let a second field, $\bar{H}_1$, which rotates with angular velocity $-\bar{\omega}$, be superimposed on the system. As viewed in the rotating frame, $\bar{H}_1$ will be stationary and the effective field becomes

$$(5) \quad \bar{H}_{eff} = \left(\bar{H}_o - \frac{\bar{\omega}}{\gamma}\right) + \bar{H}_1$$

If the coordinates are chosen such that

$$(6) \quad \bar{H}_{eff} = \left(H_o - \frac{\omega}{\gamma}\right) \bar{k} + H_1 \bar{i}$$

then $\frac{\partial \bar{M}}{\partial t}$ vanishes only for $\alpha = 90^\circ$, consequently $\frac{d\bar{M}}{dt}$ cannot vanish, and $\bar{M}$ must remain displaced with respect to $\bar{H}_o$. At resonance, $\omega_o = \gamma H_o$, $\bar{H}_{eff} = H_1 \bar{i}$, and $f_o = \frac{\omega_o}{2\pi}$ which is the Larmor precession frequency.

[3] I.I. Rabi; W. F. Ramsey; and J. Schwinger, Reviews of Modern Physics, 167, Vol 26 (1954)

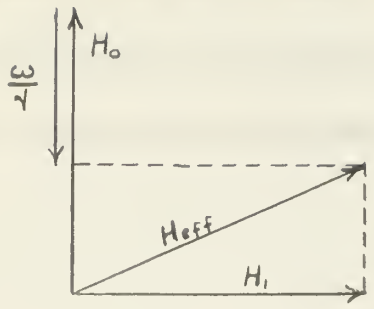

FIG. 7

EFFECTIVE FIELD IN THE ROTATING COORDINATE SYSTEM

The tipping of $\bar{M}$ represents a change in energy, ΔW, and since this is restricted to a quantum change, it remains to be shown that f_o is the frequency corresponding to the transitions discussed in section A. Neglecting second order and higher effects, and referring to the energy level diagram of the $^2S_{1/2}$ state, (Fig. 4):

(7) $W(F,m) = W_o - H_o \mu_H$ Where μ_H is the component of $\bar{\mu}_F$ in the field direction

(8) $W(F,m_i) - W(F,m_j) = -H_o \gamma\hbar (m_i - m_j)$

and since $|m_i - m_j| = 1$

(9) $|f_o| = \frac{\gamma H_o}{2\pi} = .466\, H_o\, (10^6)$ cycles/sec

In actuality, the requirement that $\bar{H}_1$ be a field rotating at angular velocity $-\omega$ is satisfied by a plane polarized wave, since a plane polarized wave can be considered to be the combination of two circularily polarized waves rotating in opposite directions. Also, $\bar{H}_1$ has thus far been assumed to be in a plane perpendicular to $\bar{H}_o$, or in the notation of the previous section, $\theta = 90^\circ$. For $\theta \neq 90^\circ$, only the component of $\bar{H}_1$ which is orthogonal to $\bar{H}_o$ is useful in inducing

transitions. The useful field, then, is given by $H_1 = H_T \sin\theta$, and the overall sensitivity of the magnetometer will have a $\sin\theta$ as well as a $\cos\theta$ orientation dependence.

C. Detection of the Precession Frequency

If the concept of a rotating set of coordinates is dropped, the rubidium vapor sample can be characterized as a total magnetization vector, $\bar{M}$, precessing around $\bar{H}_o$ at the Larmor frequency. The problem now arises as to how to detect this frequency. The most successful method thus far has been a cross beam apparatus functionally equivalent to that shown in Fig. 8.

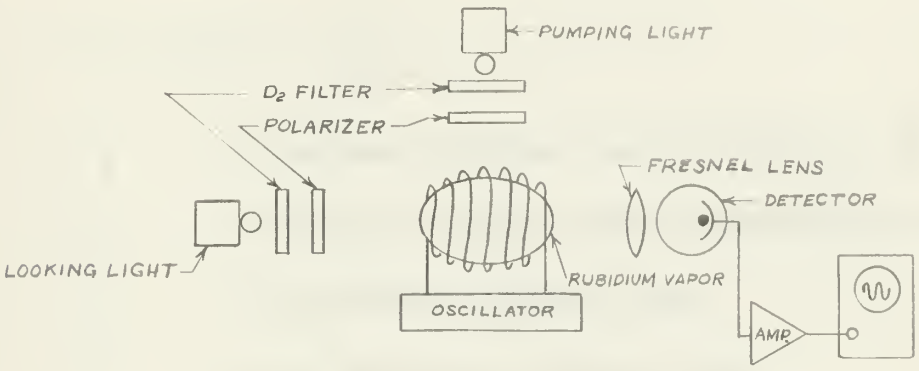

FIG. 8
CROSS BEAM DETECTION OF THE PRECESSION FREQUENCY

In a manner analogous to that of section A, it can be shown that a second circularly polarized light source with its axis in the plane of $\bar{H}_1$ will also have an effect on the rubidium sample. The sample will, in fact, be optically pumped by the second lamp; however, the transition probabilities describing the pumping action will have oscillating coefficients, thus the light reaching the photo detector will be modulated at the precession frequency. For the two energy level model, Bell and Bloom[3] have derived the following phenomenological equations for the detector output:

[3]W.E. Bell and A. L. Bloom; Phy. Rev., 107, 1560 (1957)

$$(10)\quad S_x = \frac{\gamma H_1 M_T S_2 \left[1+(S_2\Delta\omega)^2\right]^{1/2}}{1+(S_2\Delta\omega)^2+\gamma^2 H_1^2 S_1 S_2}\cos(\omega t+\psi)$$

$$(11)\quad S_z = \frac{M_T\left[1+(S_2\Delta\omega)^2\right]^{1/2}}{1+(S_2\Delta\omega)^2+\gamma^2 H_1^2 S_1 S_2}$$

where

$$S_1 = \left(P_x + P_z + \frac{1}{T_1}\right)^{-1}$$

$$S_2 = \left(P_x + P_z + \frac{1}{T_2}\right)^{-1}$$

P_z is the rate of optical pumping parallel to $\bar{H}_o$

P_x is the rate of optical pumping perpendicular to $\bar{H}_o$

T_1 is the thermal relaxation time

T_2 is the transverse relaxation time

M_T is the equilibrium population difference

At resonance the signal becomes

$$(12)\quad S_x = \frac{\gamma H_1 S_2 M_T}{1+\gamma^2 H_1^2 S_1 S_2}\cos(\omega t+\psi)$$

The system actually used in the magnetometer does not use a separate monitoring lamp but uses a single lamp offset from $\bar{H}_o$ so that the beam has components in both the X and Z directions. This means that the monitoring light, and consequently the signal intensity, will have an additional sinθ orientation dependence that must be combined with the factors previously discussed. The overall magnetometer sensitivity, as related to orientation, is given by :

$$(13) \qquad s = \frac{K \sin^2\theta \cos\theta}{1 + K^2 \sin^2\theta}$$

Fig. 9 is a plot of (13) for K=1.5.

To make the system a self oscillator the output of the photo detector is amplified and fed back to the r-f coil to produce the H_1 field.

The complete magnetometer is shown in Fig. 10.

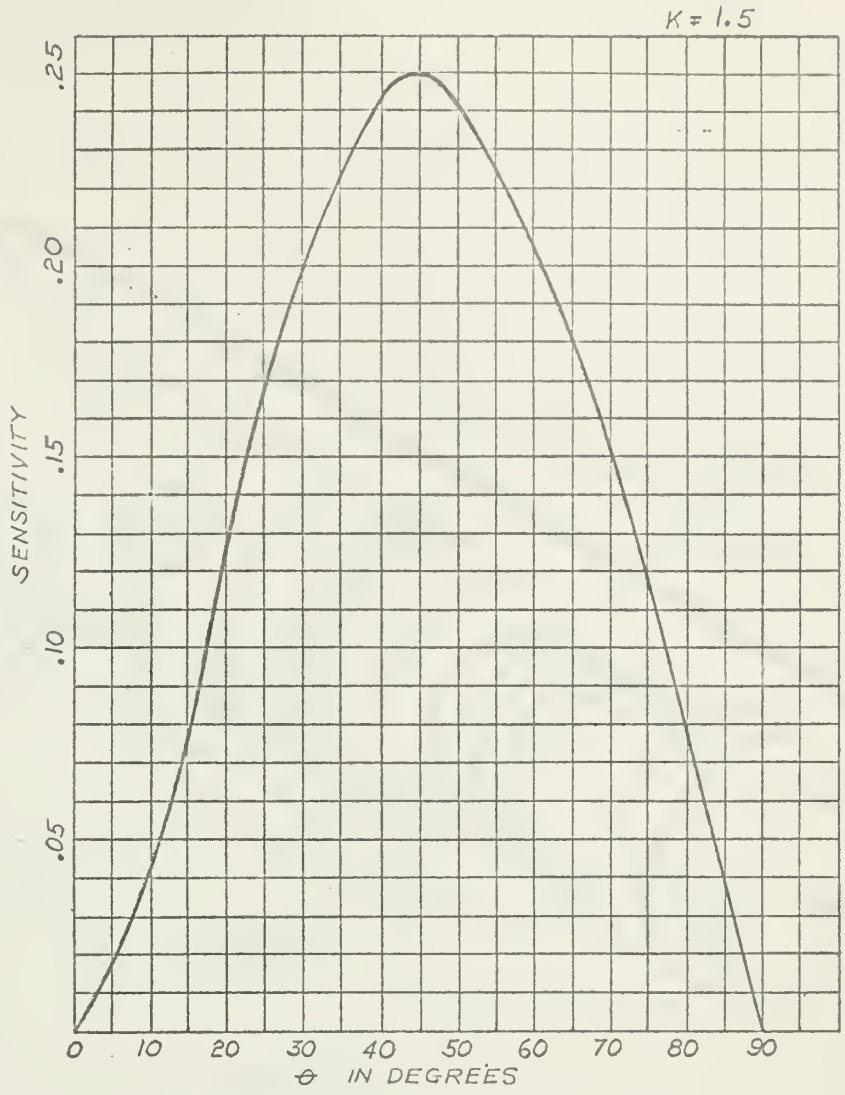

FIG. 9
MAGNETOMETER SENSITIVITY VERSUS ORIENTATION

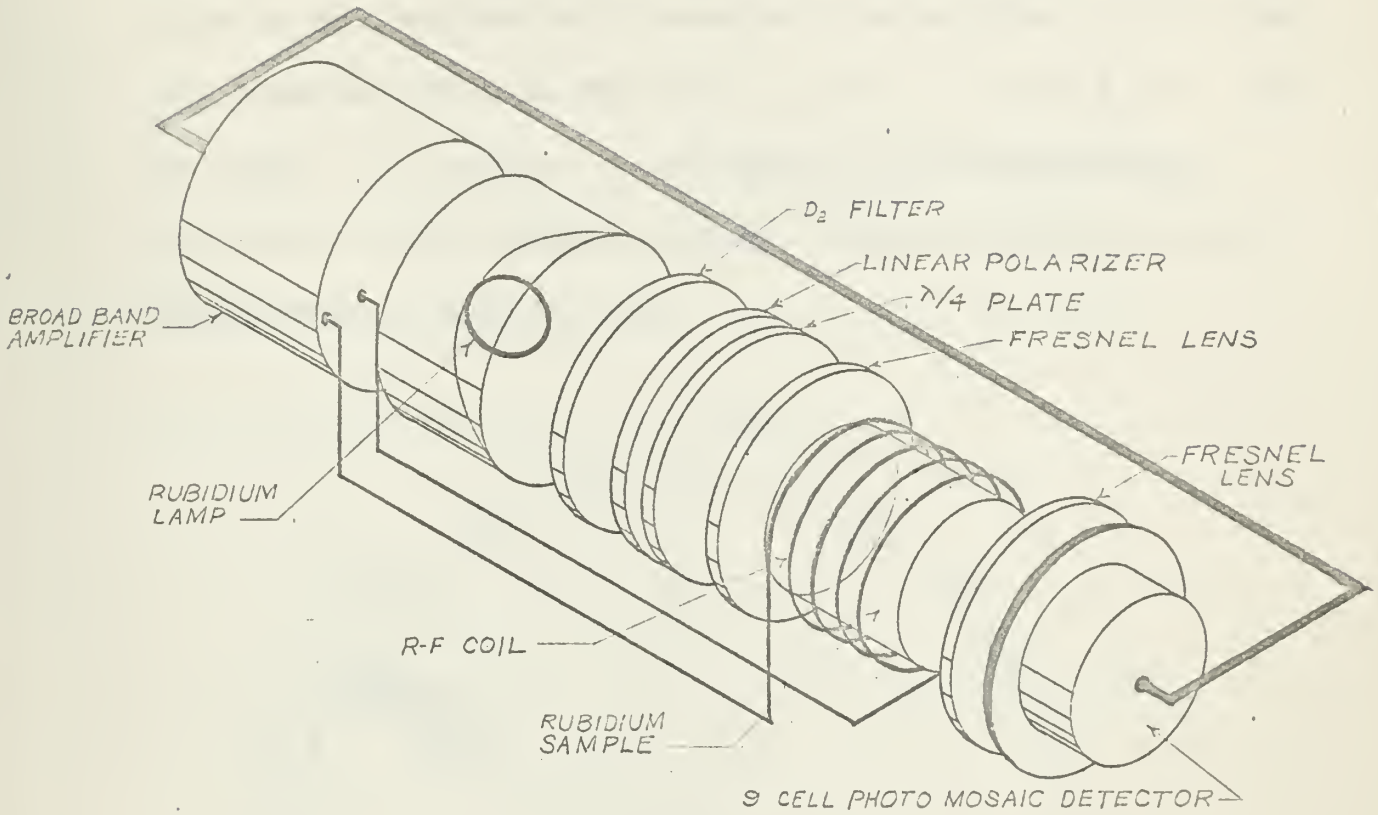

FIG. 10

CROSS-BEAM RUBIDIUM VAPOR MAGNETOMETER

III. HEADING ERROR

A. Definition of Heading Error

In this thesis the term, heading error, is defined as the difference between the oscillator frequency when the magnetometer is oriented at an angle, $\phi = \phi_o$, and when it is oriented at a second angle, $\phi = \phi_1$. The zero reference is the polar dead zone, $\phi_o = 210^\circ$. Thus $\phi - \phi_o = \Theta$, the offset from $\bar{H}_o$, however, Θ now carries a sign which eliminates ambiguities as to the direction of offset. The axis of rotation is always the East-West, or latitude, line.

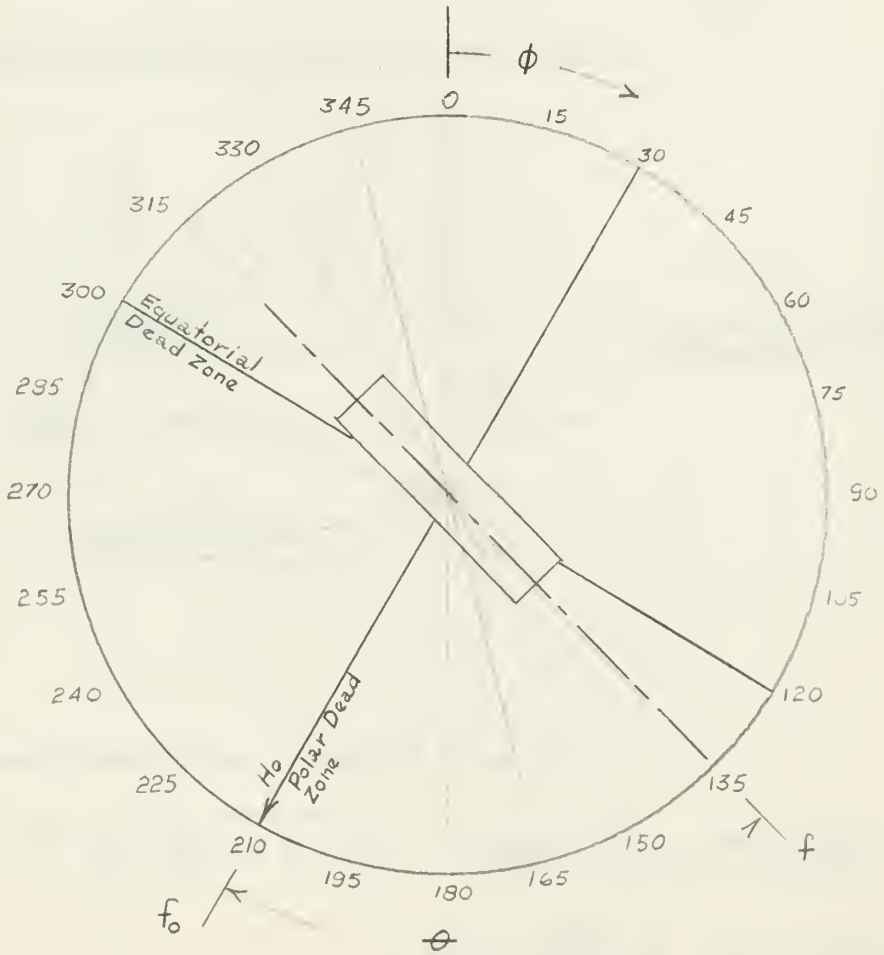

FIG. 11
EXPERIMENTAL COORDINATE SYSTEM

B. Maximum Heading Error

At present there is no analytic expression from which the exact value of heading error may be determined. Fo a given instrument the limits, or maximum heading error, however, may be calculated from the frequency spectrum obtained by a straight forward application of the Breit-Rabi equation[4]

$$(14)\quad W_{M(F,m)} = -\frac{\Delta W}{2(2I+1)} - \frac{\mu_I}{I} H m \pm \frac{\Delta W}{2}\sqrt{1+\frac{4m}{2I+1}X+X^2}$$

where $\Delta W = 2\pi\hbar\,\Delta f$ and $X = \dfrac{\left(-\mu_J/J + \mu_I/I\right)H}{\Delta W}$

An approximate plot of (14) is shown in Fig. 12.

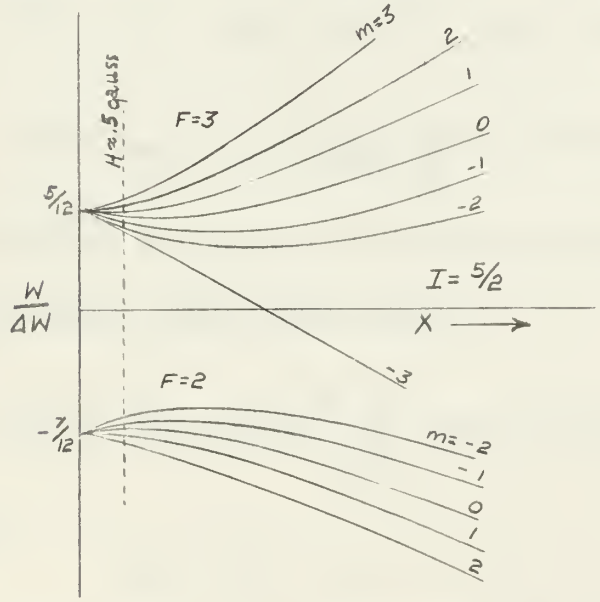

FIG. 12
VARIATION OF ENERGY WITH MAGNETIC FIELD

For small values of x, to second order

$$(15)\quad \sqrt{1+\frac{4m}{2I+1}X+X^2} \approx 1 + \frac{2m}{2I+1}\left(-\mu_J/J + \mu_I/I\right)\frac{H}{\Delta W} + \left\{\frac{1}{2} - \frac{2m^2}{(2I+1)^2}\right\}\left\{-\mu_J/J + \mu_I/I\right\}^2 \frac{H^2}{(\Delta W)^2}$$

[4] G. Breit and I. Rabi, Phys. Rev., 38, 2082 (1931)

Substituting (15) back into (14)

$$(16)\quad W_M(F,m) = -\frac{\Delta W}{2(2I+1)} - \frac{\hbar_I}{I} Hm \pm \frac{\Delta W}{2}\left[1 + \frac{2m}{2I+1}\left(-\hbar_J/J + \hbar_I/I\right)\frac{H}{\Delta W} + \left\{\frac{1}{2} - \frac{2m^2}{(2I+1)^2}\right\}\left\{-\frac{\hbar_J}{J} + \frac{\hbar_I}{I}\right\}\frac{H^2}{\Delta W^2}\right]$$

and

$$(17)\quad W_M(F,m_1) - W_M(F,m_2) = -\frac{\hbar_I}{I} H(m_1-m_2)\left\{1 \pm \frac{1}{2I+1}\right\} \mp \frac{\hbar_J/I}{2I+1} H(m_1-m_2) \pm \frac{\left(-\hbar_J/J + \hbar_I/I\right)^2}{(2I+1)^2}\frac{H^2}{\Delta W}(m_1^2 - m_2^2)$$

Using $\Delta f = 3035$ Mc/s ; $\hbar_J/J = \hbar\gamma_J = 2.79\,h\,(10^6)$; $H_o = .5$ gauss

Then

$$(18)\quad \frac{\hbar_J/J}{2I+1}(m_1 - m_2)H_o = .466\,h\,H_o = hf_o$$

$$(19)\quad f_o = .466\,H(10^6) = 233 \text{ kc/s}$$

$$(20)\quad f_{(sep)} = \left(\frac{7}{6} + \frac{5}{6}\right)\frac{H}{h}\frac{\hbar_I}{I} = 410 \text{ c/s}$$

Note that (19) is identical to the first order approximation of Part II.

Looking at the second order effects:

$$(21)\quad \left(-\hbar_J/J + \hbar_I/I\right)^2 \frac{H^2}{\Delta W}\left(m_m^2 - m_n^2\right) = 17.8\,h\left(m_m^2 - m_n^2\right) = hf_{(2nd)}$$

where

$$m_m^2 - m_n^2 = 5, 3, 1, -1, -3, -5 \quad \text{for } F = 3$$

$$(22)\qquad\qquad = 3, 1, -1, -3 \quad \text{for } F = 2$$

combining (20), (21), and (22) the resulting frequency spectrum is that shown in Fig. 13.

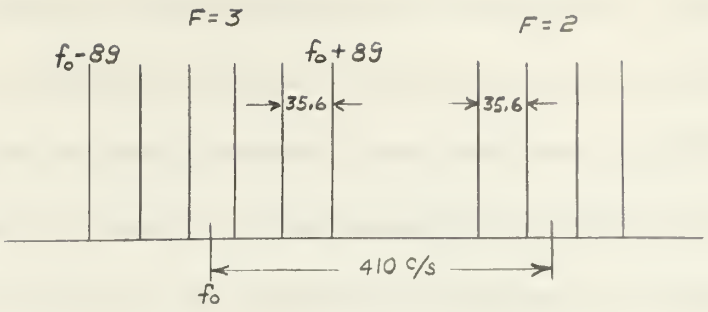

FIG.13
RESONANT FREQUENCY SPECTRUM OF Rb 85

Fig. 13 shows that the R_b 85 resonant frequency spectrum is composed of not one but ten distinct frequencies. The four lines corresponding to the F=2 transitions are of little consequence, however, as it can be shown that the intensity of these lines is small compared to those associated with the F=3 transitions.

The frequency of oscillation, then, can be expected to be some ensemble average of the F=3 spectrum. If Fig. 13 is now redrawn to show the relative line intensities when the rubidium vapor is polarized with $\Delta m=+1$ and $\Delta m=-1$ transitions, (Fig. 14), it is apparent that the frequency of oscillation will be different depending on the sense of rotation of the circularily polarized light.

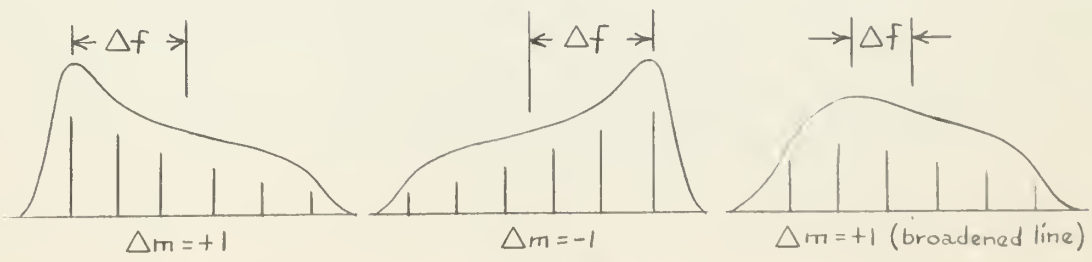

FIG. 14
RELATIVE INTENSITIES OF THE SPECTRUM LINES

Let Δf be the difference in the arithmetic mean frequency, f_o, and the frequency of the resonance line maximum. From Fig. 14 it can be seen that under conditions of complete optical pumping the frequency spectrum for F=3 would consist of only one line, $f=f_o-89$. Since Δf is, in effect, a measure of the competition between the optical pumping and the magnitude of the effective r-f feedback, it corresponds to the previous definition of heading error. The maximum heading error obtainable, therefore, is approximately 90 cycles/second. It should be noted that this value is considerably greater than that physically obtainable with this system.

C. Theoretical Values of Heading Error Versus Orientation

The consequences of Δf would not be serious if it had one value, Δf_1, throughout one hemisphere, and changed, as the magnetometer is rotated through the equatorial dead zone, to a second constant value, Δf_2. This type of error could easily be corrected by a minor adjustment of the readout equipment. Unfortunately, due to line broadening effects, Δf is not constant for any appreciable range of θ. Some of these effects have been treated analytically; however, at the present time, these treatments are for single lines and do not apply to the rotating system under consideration.

It will suffice, as far as the scope of this paper is concerned, to consider all of the line broadening effects, except the optical pumping rate and the r-f feedback, as part of the transverse and longitudinal relaxation time constants, T_1 and T_2; and then look at the resonant line shape as a function of H_1, P_x, P_z, and θ. It should be kept in mind that anything that broadens the resonance line also brings the oscillating point nearer to f_o and consequently reduces heading error.

Assuming H_1 to be a rotating field, the complete solution of the Bloch equations for the transverse component of the magnetization vector, when corrected to include optical pumping, is[5]

$$(23) \qquad M_X = \frac{1}{2} M_T \sqrt{S_2} \; \frac{S_2(\omega_o-\omega)\, 2H_1 \cos\omega t \; + \; 2H_1 \sin\omega t}{1 + S_2^2(\omega_o-\omega)^2 + \gamma^2 H_1^2 S_1 S_2}$$

[5] J. A. Pople, W. G. Schneider, and H. J. Bernstein, High-Resolution Nuclear Magnetic Resonance

where $S_1 = \left(P_x + P_z + \frac{1}{T_1}\right)^{-1}$ and $S_2 = \left(P_x + P_z + \frac{1}{T_2}\right)^{-1}$

The effect of H_1 being a linear rather than an oscillating field does not effect the validity of the solution; however, the solution now contains both in-phase and out-of-phase components with respect to the applied field, $H_1 = 2H_T \cos\theta$. These components can be described in terms of the Bloch susceptibilities, χ' and χ'' , where χ' is the in-phase component.

(24) $$M_{x_1} = 2\chi' H_1 \cos\omega t$$

and χ'' is the out-of-phase component

(25) $$M_{x_2} = 2\chi'' H_1 \sin\omega t$$

Since $M_T = \chi_o H_o$ and $\chi_o = \chi' + j\chi''$

(26) $$\chi' = \frac{\gamma}{2} M_T \frac{S_2^2(\omega_o - \omega)}{1 + S_2^2(\omega_o - \omega)^2 + \gamma^2 H_1^2 S_1 S_2}$$

(27) $$\chi'' = \frac{\gamma}{2} M_T \frac{S_2}{1 + S_2^2(\omega_o - \omega)^2 + \gamma^2 H_1^2 S_1 S_2}$$

The mean rate of absorption per unit volume is given by

(28) $$A = -M_x \, dH_x/dt$$

$$= \frac{\omega \gamma H_1^2 M_T S_2}{1 + S_2^2(\omega_o - \omega)^2 + \gamma^2 H_1^2 S_1 S_2}$$

since the $\cos\omega t \sin\omega t$ term averages to zero, and the $\sin^2\omega t$ term averages to 1/2. This shows that power is absorbed only by the out-of-phase, χ'', component. Since the magnetometer operates on the absorption mode, the signal intensity is proportional to

$$(29) \quad M_{X_2} = \frac{M_T \gamma H_1 S_2}{1 + S_2^2(\omega_o - \omega)^2 + \gamma^2 H_1^2 S_1 S_2} \sin\omega t$$

This can be obtained from equation (10) given in section II; however, now it is clear that a 90 degree phase shift is necessary in a self oscillating system, and it is possible to introduce the dispersion mode which comes from the in-phase, or χ' component.

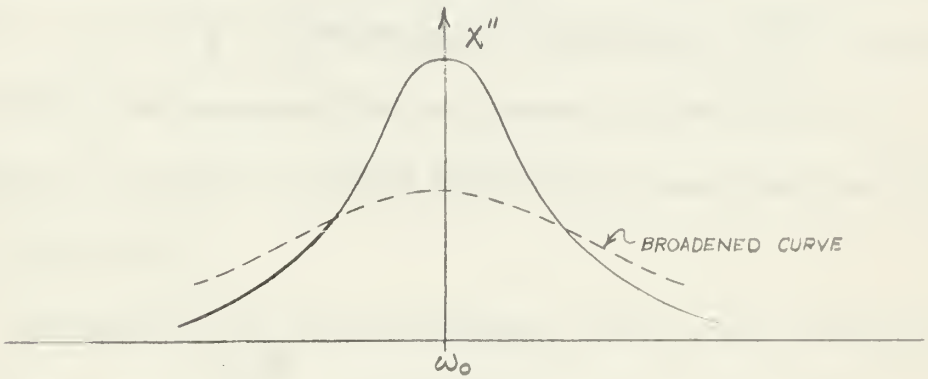

FIG. 15
ABSORPTION LINE

Fig. 15 is a plot of the absorption curve. The Lorentzian shape does not hold for the rubidium resonant line since equation (30) is valid for transitions between two lines only, however, anything which broadens this line will also broaden the rubidium line.

Using the approximation, $T_1 = T_2$, equation (29) reduces to

$$(30)\quad M_{x_2} = \frac{M_T \gamma H_1 S}{1 + S^2 [(\omega - \omega_0)^2 + \gamma^2 H_1^2]}$$

It is easily shown from (30) that the maximum value of M_{x_2} occurs for $H_1 = \frac{1}{\gamma S}$, and that $M_{x_2} = 0$ for $H_1 = 0$ or $H_1 = \infty$. The lind width is proportional to H_1. Since $H_1 = H_T \sin\theta$, and since it has been postulated that heading error is inversely proportional to line width; it can be further postulated that heading error is a function of $\{1 - |A \sin\theta|\}$ for $H_1 > \frac{1}{\gamma S}$.

The effects of $S(\theta)$ variations should not be as severe as those of $H(\theta)$ since $S = (P_z + P_x + \frac{1}{T})^{-1} = \left\{ P_{z(max)} \cos\theta + P_{x(max)} \sin\theta + \frac{1}{T} \right\}^{-1}$ and for $\frac{1}{T} \ll P_{x,z}$, the range of S would be $\frac{S}{S_o} = 1, \frac{\sqrt{2}}{2}, 1$ for $\theta = 0°, 45°, 90°$ The width of the resonance line is inversely proportional to S; therefore, if no AGC is used the heading error should also be a function of $\{1 - |B \sin 2\theta|\}$.

The heading error versus orientation curve for the absorption oscillation, then, can be expected to be similar to Fig. 16. Fig. 17 is a plot of the dispersion curve. By utilizing the appropriate phase shift, 0 or 180°, the magnetometer can be made to oscillate on either of the two peaks. These peaks now occur at a frequency, ω, for which $H_1 = \frac{\sqrt{1 + S^2 (\omega - \omega_0)^2}}{\gamma S} \approx \frac{|\omega - \omega_0|}{\gamma}$. Thus the frequency separation of the maxima is directly proportional to the magnitude of H_1. As H_1 is decreased the dispersion oscillation frequency does not reduce to f_o but to the absorption frequency. This means that the heading error will

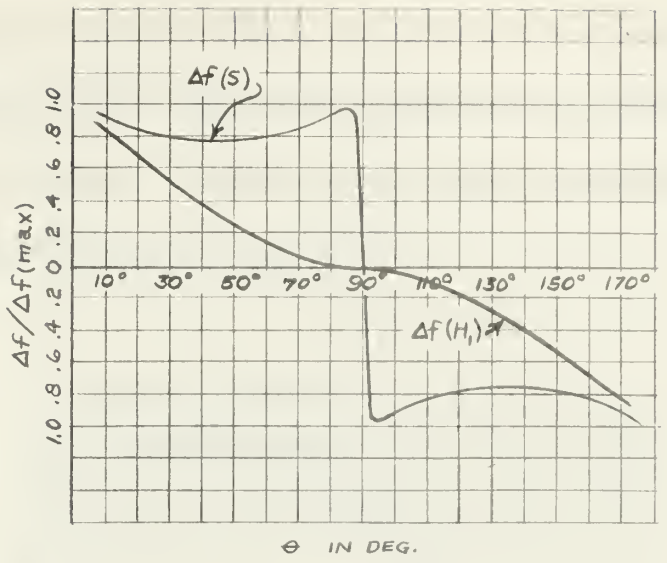

FIG. 16
POSSIBLE HEADING ERROR VERSUS ORIENTATION FOR THE ABSORPTION OSCILLATION

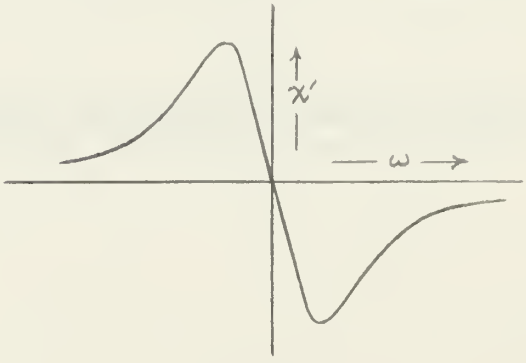

FIG. 17
DISPERSION LINE

not be symmetrical about the equatorial dead zone. There may even be an optimum choice of H_T such that as the instrument orientation is varied throughout one hemisphere, the effects of H_1 on line broadening and the dispersion peaks separation cancel and the heading error will be essentially constant. A heading error versus orientation plot could conceivably be that shown in Fig. 18.

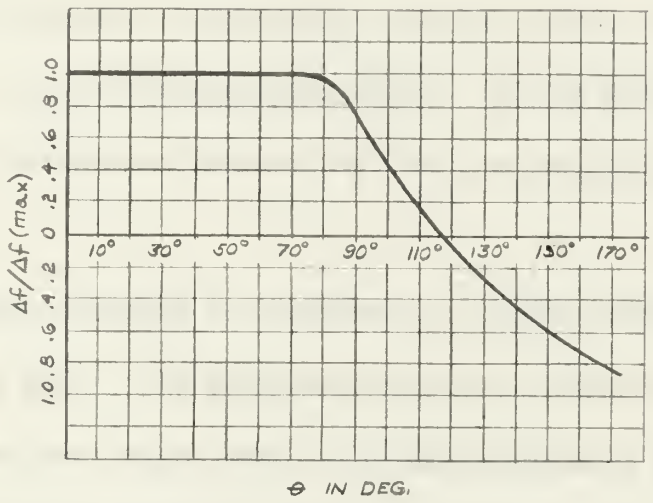

FIG. 18

POSSIBLE HEADING ERROR VERSUS ORIENTATION FOR THE DISPERSION OSCILLATION

IV. EXPERIMENTS

A. Polarizer Rotation

In the experiments to follow, a 180° rotation of the magnetometer was simulated by changing the polarity of the pumping light. This has several advantages: (1) The effects of magnetic components in the system are minimized. (2) The light polarity can be changed in a fraction of the time necessary to rotate the entire system, thus the effect of field variations is minimized. (3) The system components can be assembled in more accessible locations. (4) The necessity to manually switch the r-f connections when going from one hemisphere to another is eliminated.

The circular polarizer is composed of a linear polarizer followed by a quarter- wave plate. The polarizer and quarter-wave plate are aligned such the quarter-wave plate sees two equal components of linearly polarized light, one of which is passed unaltered, the other delayed 90°. The polarity of circular polarization is changed by a 90° rotation of either the linear polarizer or the quarter-wave plate.

The reason that the sense of rotation of H_1, does not have to be reversed in order to maintain an oscillation when the light polarity is reversed is easily explained with reference to the classical vector model.

Fig. 19a shows the instantaneous position of the angular momentum vector, $\bar{F}$, when $2H_1 \cos\omega t = 2H_1$. For $\Delta m = +1$, $\bar{\mu}_F$ is oppositely aligned with respect to $\bar{F}$; thus the precession and tipping torques given by $\bar{L}_1 = \bar{\mu}_F \times \bar{H}_o$ and $\bar{L}_2 = \bar{\mu}_F \times \bar{H}_1$, result.

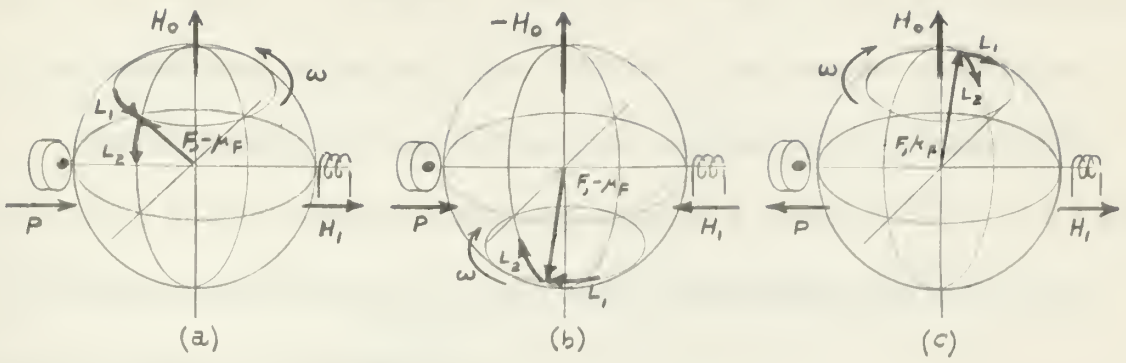

FIG. 19

PHASE RELATIONSHIPS IN THE SELF-OSCILLATING MAGNETOMETER

Fig. 19b shows $\bar{H}_0$ reversed. Now in order to produce a tipping torque and still maintain the 90° phase lag necessary for oscillation, it is evident that the polarity of $\bar{H}_1$ must be reversed.

In Fig. 19c, the polarity of light is reversed instead of $\bar{H}_0$. Optical pumping now is in the negative energy direction and tends to align $\bar{\mu}_F$ with $\bar{H}_0$; however, $\bar{\mu}_F$ is also aligned with $\bar{F}$ since $\Delta m = -1$, and the net result is a reversal of precession direction. The conditions for oscillation, then, are maintained without changing the polarity of $\bar{H}_1$.

B. Experimental System

The components illustrated in Fig. 10 were enclosed in a cylindrical, aluminum container, a section of which was removed to allow free access to the components and to facilitate rotation of the quarter-wave plate.

The temperature of the gas cell was maintained at approximately 40° C by a 60 cycle heater which consisted of a bifilar winding of 5 turns of nichrome wire wound over the r-f coil. A calibrated thermistor was used to moniter the temperature.

The complete system mounted on a wooden rotatable platform is shown in Fig. 20.

FIG. 20
EXPERIMENTAL APPARATUS

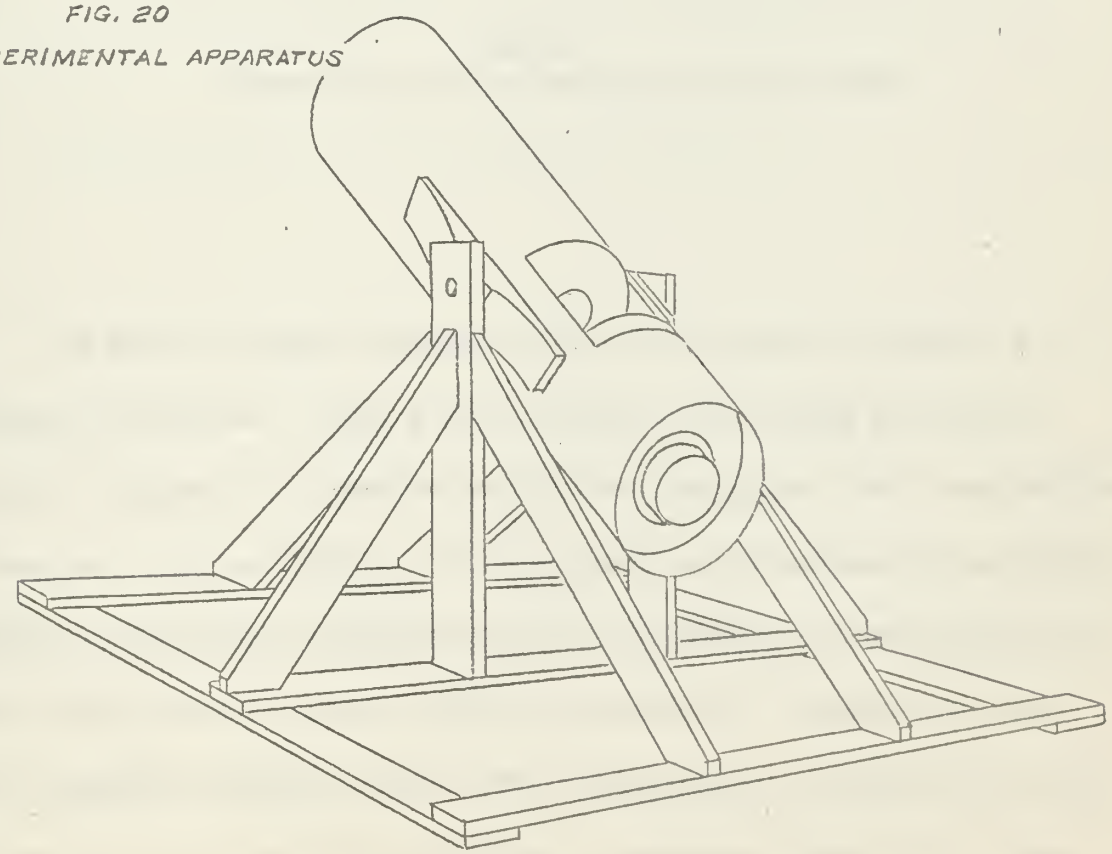

C. Line Shape

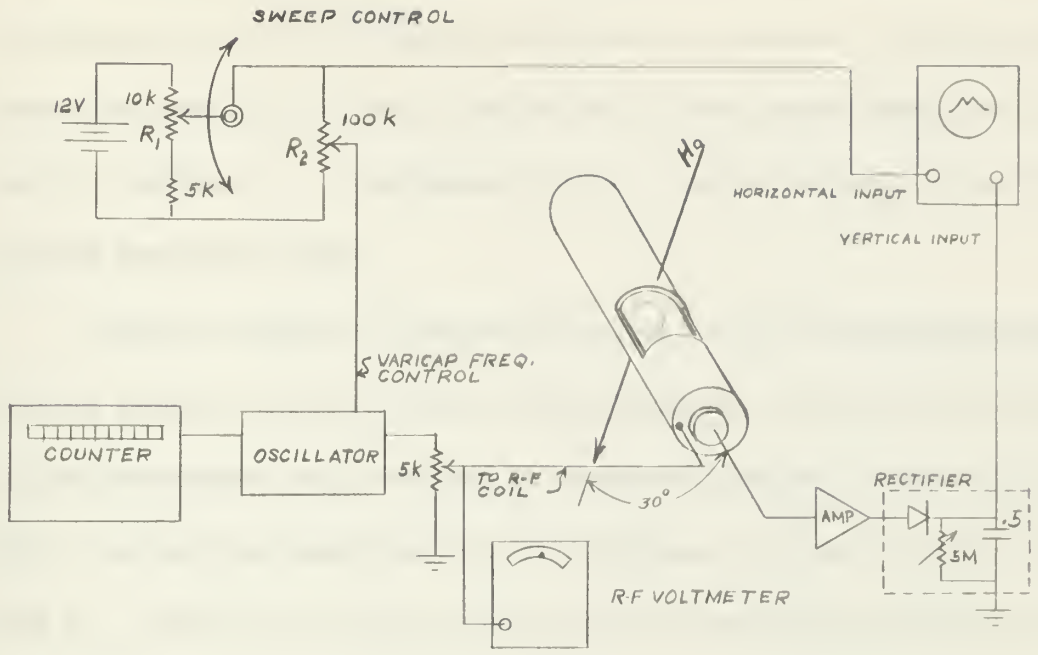

FIG. 21
EXPERIMENTAL SET UP FOR OBTAINING LINE SHAPE

The driven system diagramed in Fig. 21 was used to obtain the resonant line shape. Unlike a self-oscillator, the output of a driven system is neither the dispersion nor the absorption line, but a combination of the two. This is possible since the phase angle between the externally applied r-f field and the detector output is not fixed, but varies with frequency such that the detector output is a maximum. Although this prevents desirable absorption band width measurements, it does give useful information in that the absorption line is predominant when the r-f level is below the saturation value while the dispersion line is predominant

for values of r-f above the saturation level.

A 15 to 20 second linear sweep was used to drive both the scope horizontal input and the varicap controlled oscillator. The sweep was generated manually, using a line and pully arrangement attached to a ten turn helipot, R_1. The second pot, R_2, was adjusted to obtain the desired frequency sweep.

The line shapes for various values of r-f drive were photographed using a polaroid camera set for a time exposure. Frequency calibration of the photographs was obtained by disconnecting the scope vertical input, moving the remaining spot to significant positions on the scope with R_1, and making multiple exposures to record these positions on the photograph while recording the frequency corresponding to each spot position.

Representative results are shown in Fig. 22.

FIG. 22
RESONANCE LINE SHAPE AS A FUNCTION OF
R-F DRIVE

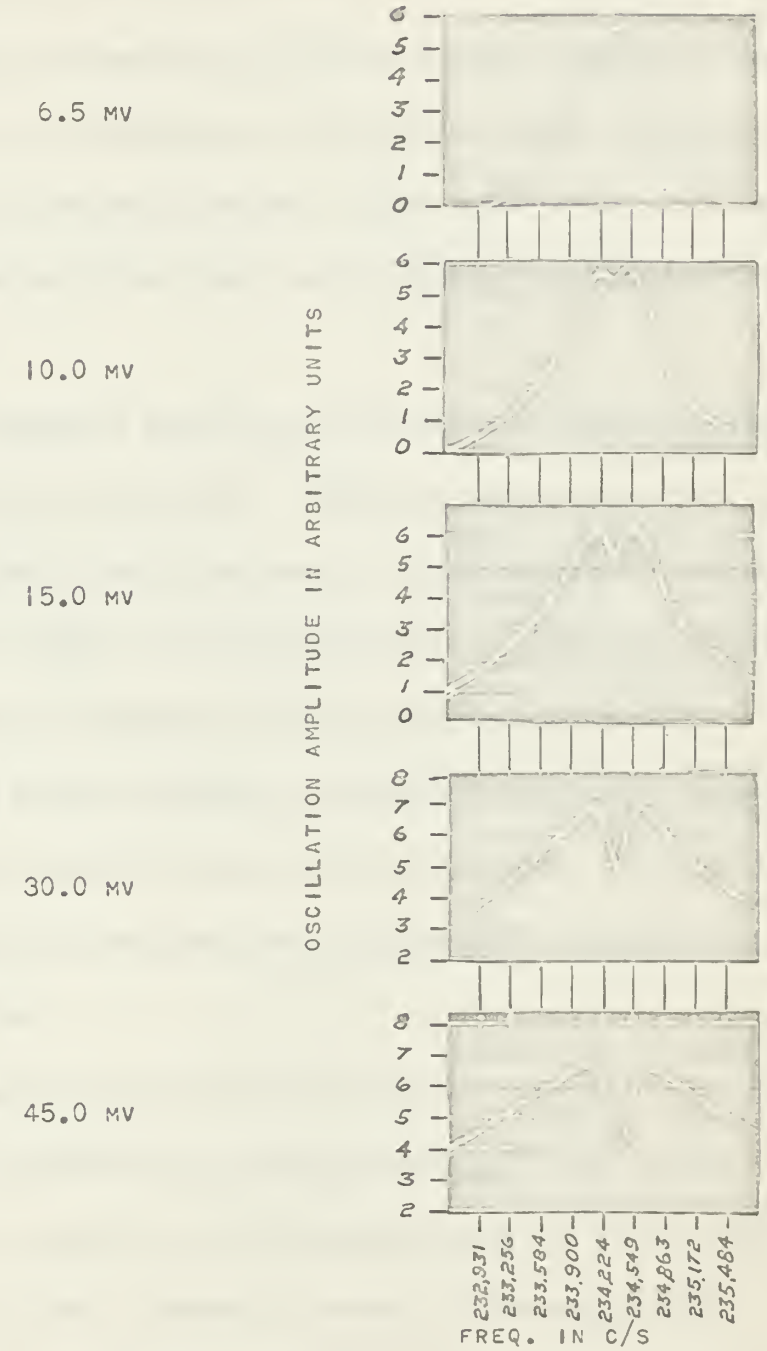

D. Heading Error Versus Phase Angle

A determined effort was made to measure the phase angle between the output of the detector and the input to the r-f coil. Since the photocell gives the 90 phase lag necessary for the absortion oscillation, and since the ratio of the coil impedance to the amplifier output impedence is on the order of 1/50; this measurement, added to 90, would have been a very good approximation of the phase angle between the light intensity and the r-f field, Hl.

A comparator capable of measuring phase shifts of approximately $\pm 5^{\circ}$ was designed and constructed. Although bench tests of the device were satisfactory, it would not work in the experimental magnetometer system. In the light of later developments, it appeared that the most probable reason for its failure is that an external phase shifter, used to obtain a good strong oscillation, produced an additional 90 shift which was completely beyond the range of the comparator. The signal thought to be the absortion oscillation was subsequently identified as a dispersion oscillation.

The system finally used was the self-oscillator shown in Fig. 23. The desired mode of oscillation was selected with the $0-180^{\circ}$ active phase shifter, and the phase was varied approximately 13° either side of the oscillating point with a series L-C network. The amplitude of the r-f input was held to 5mv by varying the output level of the active phase shifter to compensate for the drop across the L-C circuit.

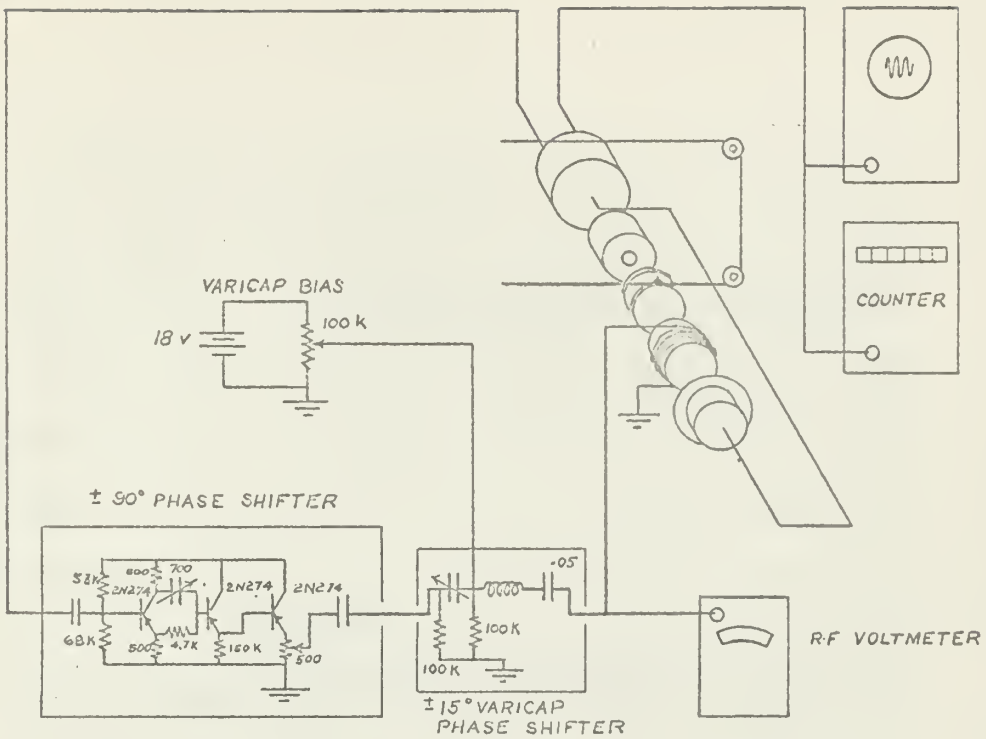

FIG. 23
EXPERIMENTAL SET UP FOR OBTAINING PHASE ANGLE AND ORIENTATION EFFECTS

FIG. 24
VARICAP PHASE SHIFTER CALIBRATION CURVE

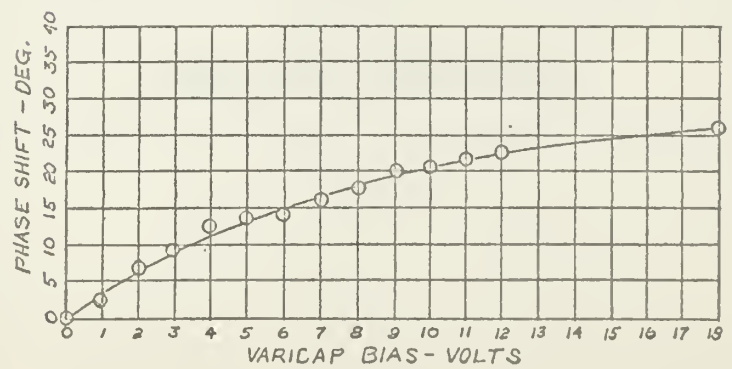

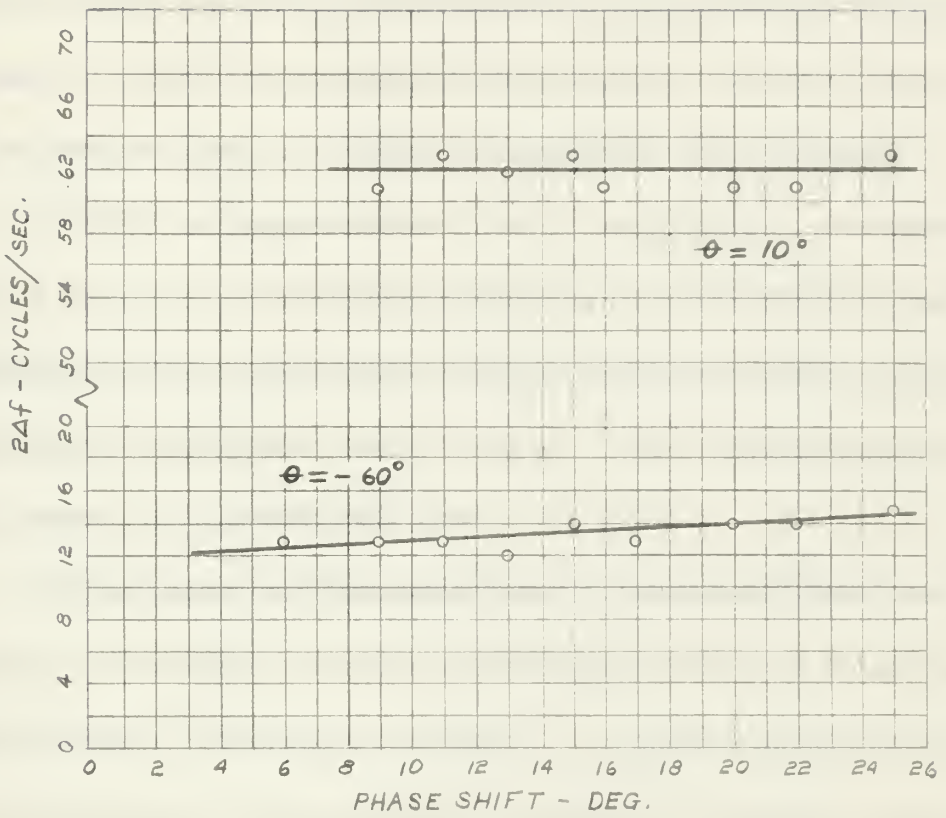

FIG. 25

PHASE SHIFT VERSUS 2Δf

E. Heading Error Versus Orientation

Although the present magnetometers are not designed to oscillate at the dispersion peak, it was found that by inserting an additional 90° phase to either cancel the 90° introduced by the photocell detector or increase it to 180°, an oscillation was obtained. To verify that this was the dispersion mode, the following experiment was performed:

(1) With the magnetometer initially oscillating at a suspected dispersion peak, the r-f drive was reduced until the oscillation ceased. Depending on the magnetometer orientation, the minimum r-f level necessary for oscillation was 5 to 10 mv. The r-f drive was then reduced still further, to approximately 1mv.

(2) The phase was then varied until a weak oscillation was again obtained. The phase shift was approximately-90°, thus it was assumed that this was an absorption oscillation. To check, the phase was held constant and the r-f level gradually increased. The signal amplitude increased to a saturation point and then decreased. The r-f level was further increased until the oscillation either completely disappeared or, in some cases, reduced to a violent squegging.

(3) The r-f was held constant and the phase angle shifted +90°, to its original value. A strong oscillation about 200 cycles/sec higher than the absortion oscillation frequency was observed.

Since the results of (1), (2), and (3) coincide with those predicted by the Bloch equations, it was concluded that it was possible to obtain both dispersion and absortion mode oscillations.

Data was obtained to determine the heading error for both modes of oscillation. The experimental system and procedure was the same as that used to obtain the heading error-phase relationship, except that the magnetometer was rotated and the phase held constant. The frequency difference observed by rotating the circular polarizer is taken as $2\Delta f$; i.e., it is assumed that heading error is symmetric about the equatorial dead zone.

The results of this experiment are tabulated in Fig. 26. No inferences should be drawn from direct comparisons of oscillating frequencies at different magnetometer orientations. The magnetic field gradient in the room in which this experiment was conducted was so severe that it was found necessary to use a small compensating field to obtain a satisfactory absorption oscillation, and the amount of compensation was not necessarily the same for all orientations. Care was taken, however, to insure that the total field vector at the absorption cell remained fixed at .

FIG. 26
TABULATED VALUES OF Δf VERSUS ORIENTATION

MODE	ϕ in deg.	θ in deg.	$f_{(max)}$ cycles/sec.	$2\Delta f$ cycles/sec.	DRIVE volts rms.
A	150	-60	234,274	15	3.5 (10^{3})
			260	12	4.0
D			446		12.0
			472		13.0
A	160	-50	234,298	47	1.4
			276	40	2.0
			250	34	2.5
			222	27	4.2
D			493	13	50.0
			432	15	30.0
			394	10	20.0
A	170	-40	234,835	59	3.0
			860	51	3.8
			871	47	4.1
D			235,177	40	20.0
			189	20	30.0
			345	23	100.0
A	180	-30	234,218	40	5.0
			217	36	10.0
			235	30	11.0
D			643	37	20.0
			666	34	29.0
A	190	-20	234,230	52	5.0
			225	36	10.0
			219	25	15.0
D			378	8	21.0
			364	19	10.0
A	220	10	234,138	63	5.0
			127	46	10.0
			116	36	14.0
D			294	31	20.0
			310	23	29.0
A	230	20	234,154	64	5.0
			145	42	10.0
			145	33	13.0
D			304	26	20.0
			311	22	30.0
			313	22	34.0

MODE	ϕ in deg.	θ in deg.	f(max.) cycles/sec.	$2\Delta f$ cycles/sec	DRIVE volts r.m.s
A	240	30	234,198	63	1.0 (10^{-3})
			181	50	5.0
			159	36	7.0
			146	26	10.0
			150	15	15.0
D			363	23	20.0
			414	20	30.0
			656	21	80.0
A	250	40	234,963	41	5.0
			960	18	10.0
D			235,200	26	10.0
			208	22	20.0
			223	27	30.0
A	260	50	234, 352	28	5.0
			341	21	6.0
				16	7.0
A	270	60	234, 341	16	5.0
			336	12	8.0
			325	10	10.0

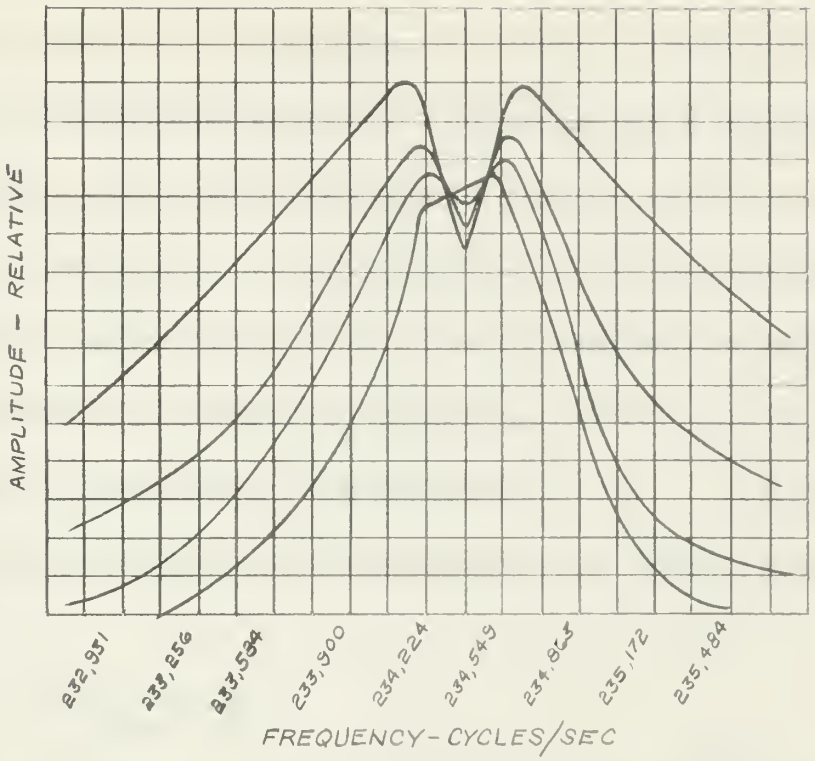

FIG. 29
RESONANCE LINE SHAPE

Fig. 27 is a composite of the individual line shapes shown in Fig. 22. As previously mentioned, it is not possible to separate the absorption and dispersion lines; however, since a pure dispersion line has a null at $\omega = \omega_o$, the peak of the absorption is the minimum of the trough between the two dispersion peaks. The experimental results agree with those predicted by the Bloch susceptability components. This leads to the conclusion that calculations based on only two energy levels are sufficiently accurate to represent the actual system, and adds a measure of confidence to the extension of these calculations in predicting heading error.

The graph shown in Fig. 25 is deceiving in that it suggests that there is no heading error dependence on the phase angle between the monitoring light and coil excitation. For sufficient broadening, the absorption line shape is practically symmetrical about the line peak; consequently, introduction of a phase of other than -90° causes the frequency of oscillation to shift to one side of the line maximum. If this shift is, say +25 cycles/sec., then by changing the polarity of circular polarization a frequency difference, $(\Delta f - 25) + (\Delta f + 25) = 2\Delta f$ is obtained Thus, although the plotted data, $2\Delta f$, is independent of phase, no conclusions can be extrapolated for heading error.

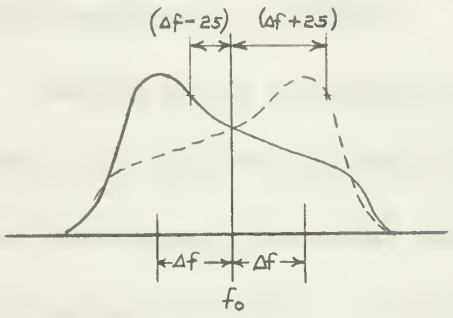

FIG. 23

EFFECT OF PHASE SHIFT ON HEADING ERROR

In an operating magnetometer the phase angle between the light if fixed at -90°; therefore little valuable information is lost in the experimental procedure. Of major importance is the fact that phase effects can be discounted in the results of the primary experiment - heading error versus orientation.

It has been assumed that the principal line broadening factor is the magnitude of H_1 . If a relatively large value of H_T is selected,

and this value held constant as the magnetometer is rotated, since $H_1 = H_T \sin\theta$, the heading error should vary as $\Delta f = \Delta f_{(max)}\{1-|A\sin\theta|\}$ Fig. 30 is a plot of Δf versus θ for $H_T = 5$ mv. For large values of θ it was necessary to extrapolate the value of Δf by extending a $\Delta f - rf\big|_{\theta=0}$ plot to an r-f value of 5 mv.

The effect of the optical pumping factor $|P_z + P_x|$, on heading error is shown in Fig. 31. This graph is the result of varying the orientation while holding H_1 constant. Again, the incremental values of were picked off of the $\Delta f - rf\big|_{\theta=0}$ plot.

Figs. 28 and 29 are similar to the curves predicted in section III, although it is obvious that the simple relationships stated do not adequately represent the system.

Another factor that cannot be explained at this time is the relation between H_1 and the oscillating frequency. Referring to Fig. 26, in most cases the frequency recorded was the higher of the frequencies for the two polarizer positions. It is logical that as the r-f drive is increased, the line is broadened, and the oscillating frequency should decrease toward f_o. If the theory of section III is correct, this decrease in frequency should be one half the decrease in $2\Delta f$. This is not the case. For $\theta = -50°$, the change in heading error is 10 cycles while the change in oscillating frequency is 72 cycles. For $\theta = -20°$, the change in heading error is 13 cycles for an oscillating frequency change of 11 cycles. This would seem to suggest that, since for larger values of θ, H_1 is more nearly equal H_T, there is some interaction between the field being

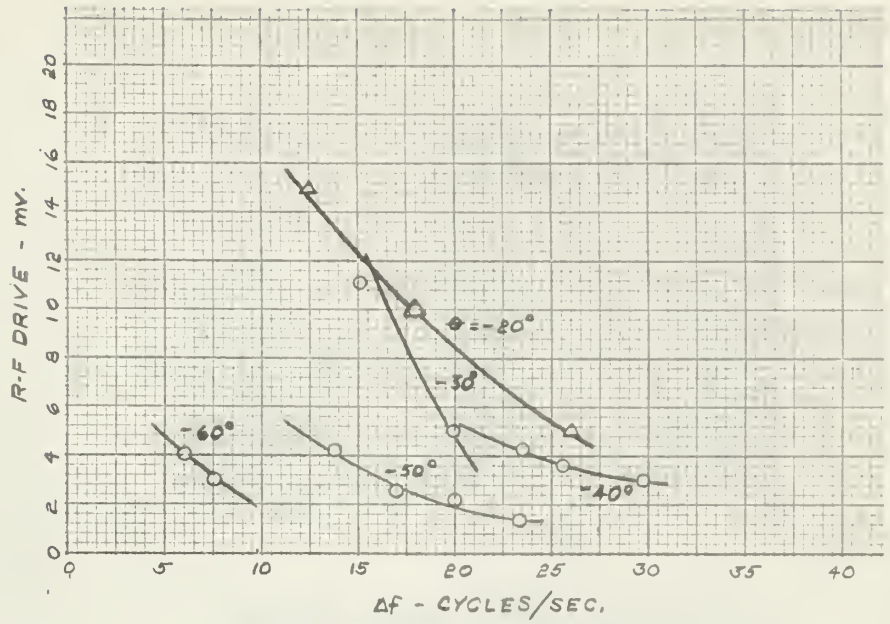

FIG. 29

HEADING ERROR VERSUS ORIENTATION

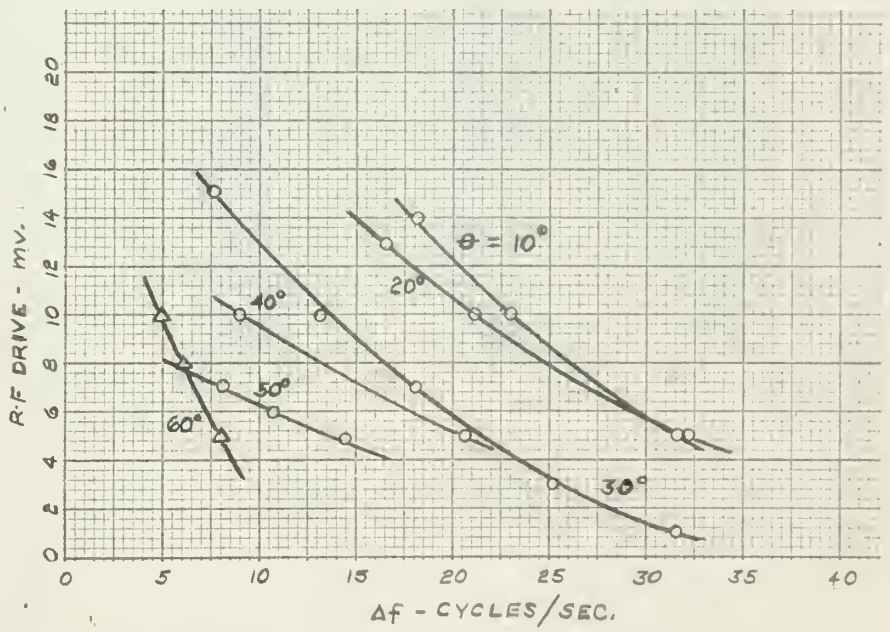

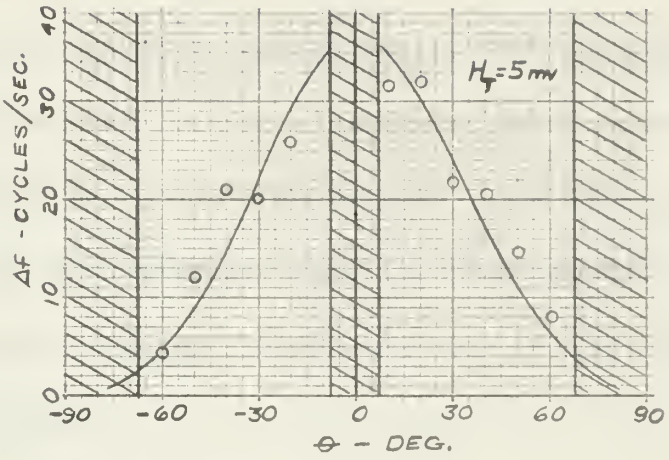

FIG. 30
HEADING ERROR VERSUS ORIENTATION
WITH H_T HELD CONSTANT

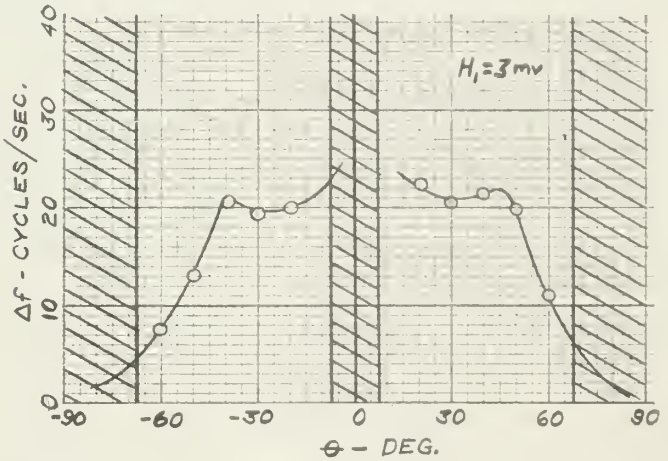

FIG. 31
HEADING ERROR VERSUS ORIENTATION
WITH H_1 HELD CONSTANT

measured and the oscillating r-f field.

Data relating to the dispersion oscillation does not plot in any significant pattern. Unfortunately, the primary emphasis of these experiments was the absorption mode, consequently, the data taken using the dispersion oscillation was sketchy. The general trend, however, both in the data recorded and in many observations which were not recorded, is that heading error is considerably less for the dispersion oscillation. This goes along with the theory that heading error is reduced by an increase in the r-f field.

VI. CONCLUSIONS

The theoretical development and experimental results both show significant effects of orientation on the oscillating frequency of the magnetometer, and although only the system using Rb^{85} was investigated, the theory indicates that this will be the case for any system using an absorption media having nuclear spin other than zero.

To obtain an orientation insensitive instrument, the first thought is to use metastable helium which, like the alkali vapors, is characterized by a single electron in the outer shell, but unlike the alkali vapors, does not have nuclear spin. This solution has several disadvantages. First, the high potential necessary to excite the helium to the metastable state gives rise to additional sources of error such as the Stark effect. Secondly, for a magnetic field of .5 gauss, the Larmor precession frequency of metastable helium if 1.4 megacycles which is considerably higher than the frequency response of present photo-detectors. This means that complex detection schemes must be devised and the result is a more complicated system. There are other problems connected with the helium magnetometer, but the purpose here is just to show that a switch to helium to eliminate the orientation effects inherent in rubidium is probably not the optimum solution.

Since heading error in the rubidium magnetometer does follow a definite pattern which, with a little more experimentation, can be defined quite precisely, there should be feasible methods by which it can be reduced to acceptable limits.

One of these methods presently being studied at Varian is the use of multiple cell systems. This not only reduces the heading error, but also eliminates the polar and equatorial dead zones associated with the single cell unit.

Another possible solution is to build an orientation sensitive phase shifter which automatically adjusts the oscillating point on the absorption line to compensate for any frequency shift due to magnetometer orientation. This could be accomplished by a sophisticated switching and discriminator arrangement that would sample each of the dispersion frequencies and produce a d-c voltage proportional to the difference frequency, which, in turn, would be compared to a d-c voltage proportional to the r-f input to the feedback coil. The error voltage thus produced would be a function of the magnetometer orientation since the separation of the dispersion peaks is directly related to the component of $\bar{H}_T$ perpendicular to $\bar{H}_o$. The error voltage, then, could be applied to a varicap controlled phase shifter which would change the oscillator frequency to the correct value.

Still another solution might be to artificially broaden the absorption line by adding additional impurities to the rubidium vapor. This, however, may not be a wise choice in that it is equivalent to adding noise to the system and would deteriorate the performance of the instrument.

Further experimentation will quite possibly produce data that will suggest better ways of reducing heading error than those just discussed. With this in mind, it may be beneficial to mention some additional experiments that the writer feels are essential to a thorough understanding of the problem.

1) The assumption that heading error is symmetrical about the equatorial dead zone must be verified. This may be done by mounting the magnetometer is a non-magnetic cradle and the oscillation frequency observed as the entire system is rotated 360°. This is not a simple experiment in that the most carefully designed cradle will cause some distortion of the magnetic field, and even these small distortions can be significant when compared to the 10^{-7} gauss sensitivity of the instrument.

2) The effect of phase shift on the oscillation frequency should be determined. Again, this is not a simple problem. First it must be shown that the assumptions of 90° phase shift in the photo cell and negligible phase shift in the r-f coil are valid, and then a phase measuring device designed that will measure the phase difference between the photo detector output, (approx. 10^{-7} volts), and the input to the r-f coil, (approx. $5\ 10^{-3}$ volts).

3) When the comparatively large effects of r-f drive and phase shift are known and can be isolated, then smaller effects, such as those caused by light intensity and absorption cell temperature, can be investigated.

This final section was written under the assumption that it is desirable to make the magnetometer completely orientation insensitive. This is not intended to convey the impression that the rubidium magnetometer is not a very useful instrument regardless of heading error. Actually there are applications where useful information, such as the

rate of rotation of a satellite, can be obtained by making use of the orientation sensitive characteristics inherent in a rubidium device.

BIBLIOGRAPHY

1. A. Kastler, Proc. Phys. Soc., A67, 853 (1954)

2. G. Herzberg, Atomic Spectra and Atomic Structure, Dover Publications, New York, N. Y., 1944

3. W. E. Bell and A. L. Bloom, Phys. Rev., 107, 6, 1559 (1957)

4. G. Breit and I. Rabi, Phys. Rev., 38, 2082 (1931)

5. J. A. Pople, W. G. Schneider, and H. J. Bernstein, High-resolution Nuclear Magnetic Resonance, McGraw-Hill, New York, N. Y., 1959.